Proc. Natl. Acad. Sci. USA
Vol. 78, No. 7, pp. 4319–4323, July 1981
Biophysics

Three-dimensional structure of the complex of skeletal muscle actin and bovine pancreatic DNase I at 6-Å resolution

(F-actin filament/crystal structure/x-ray diffraction)

DIETRICH SUCK*, WOLFGANG KABSCH†, AND HANS GEORG MANNHERZ‡

*European Molecular Biology Laboratory, Postfach 102209, D-6900 Heidelberg, Federal Republic of Germany; †Max-Planck-Institut für medizinische Forschung, Abteilung Biophysik, Jahnstrasse 29, D-6900 Heidelberg, Federal Republic of Germany; and ‡Institut für Anatomie und Zellbiologie der Universität, Robert-Koch-Strasse 6, D-3550 Marburg, Federal Republic of Germany

Communicated by John C. Kendrew, April 8, 1981

ABSTRACT **The structure of rabbit skeletal muscle actin complexed with bovine pancreatic DNase I has been determined by x-ray crystallographic methods at 6-Å resolution. The analysis was based on a new orthorhombic crystal form, space group $P2_12_12_1$, with one complex in the asymmetric unit. Six isomorphous heavy-atom derivatives yielding an overall figure of merit of 0.72 have been used to calculate the electron-density map. Molecular models for actin and DNase I derived from this map have dimensions 67 × 40 × 37 Å and 50 × 50 × 40 Å, respectively. The actin molecule is elongated and consists of a larger and a smaller domain, each containing density regions resembling a central β-pleated sheet surrounded by α-helices. The highest electron-density peak is found in the cleft between the two domains, perhaps indicating the bound ATP. Observed crystal contacts between actin molecules and a model for the F-actin filament are discussed. Two high-affinity Ca^{2+}-binding sites which also bind Ba^{2+} have been located at the surface of the DNase I molecule.**

In addition to muscle tissues, where it forms the backbone of the thin filament, actin-like proteins have been shown to occur in every eukaryotic cell so far examined (for review, see refs. 1 and 2). The complete amino acid sequence of rabbit muscle actin has been determined (3) and comparative sequence analysis data (4) have shown that actins from various sources differ by only a small number of conservative amino acid exchanges predominantly at the NH_2 terminus, thus emphasizing its highly conserved primary structure (4).

The classical function of actin is the formation of force-producing crosslinks with myosin heads (for review, see ref. 5), a function that actin can perform only in its polymerized form, F-actin. In nonmuscle tissues, a larger percentage of the actin appears to exist in its monomeric form, G-actin, representing a pool from which it is believed to be transformed into the filamentous form on demand. The degree of polymerization is supposed to be regulated by proteins able to interact with actin.

Besides the classical contractile proteins such as myosin, tropomyosin, and troponin, the list of proteins actin is able to interact with is vast and still growing. Most of these proteins exhibit strong affinity to filamentous actin, but only two interact firmly with monomeric actin, profilin and DNase I (6–8).

Actin and DNase I form a stoichiometric 1:1 complex with high affinity ($K_B = 5 \times 10^8\ M^{-1}$ (9). Addition of equimolar concentrations of DNase I to F-actin leads, within minutes, to complete depolymerization of the latter by formation of the actin·DNase I complex and to functional inhibition of both proteins (7, 8)—i.e., the enzymatic activity of DNase I and the ability of actin to polymerize in the presence of high salt. The physiological significance of this interaction is still obscure, although the natural occurrence of an actin·DNase I complex could be demonstrated in rat pancreatic juice (10).

DNase I is generally regarded as a digestive enzyme secreted by the exocrine pancreas; similar activities, however, have been reported to occur in a number of eukaryotic cells (11). Native double-stranded DNA is most effectively hydrolyzed, leading to the formation of single-stranded 5′-oligonucleotides. The complete amino acid sequence of its single peptide chain is known (12). Four cysteines form two intramolecular disulfide bridges; one of these bridges is essential for its enzymatic activity. A carbohydrate chain of varying length and composition, giving rise to four isoenzymatic forms (13), is covalently linked to asparagine at position 18.

MATERIALS AND METHODS

Protein Preparations. DNase I was from Worthington and was further purified by chromatography on hydroxyapatite as described (9). Rabbit skeletal muscle actin was prepared from dry acetone powder (9) including two cycles of polymerization and depolymerization. Chicken gizzard actin was prepared as described (14).

Actin·DNase I complex was formed by mixing purified actin and DNase I at equimolar concentrations for 1 hr at room temperature. Uncomplexed material was removed by chromatography on a AcA 44 (LKB) column (45 × 2.5 cm) equilibrated with 0.2 mM ATP/0.1 mM $CaCl_2$/0.5 mM NaN_3/0.1 M imidazole, pH 6.8.

Crystals. Crystallization was carried out, at 4°C and room temperature, from buffered protein solutions at pH 6.6 by adding 8–10% polyethylene glycol 6000 as precipitating agent. Two different buffer solutions were used: buffer A, 50 mM imidazole/0.1 mM $CaCl_2$/1 mM NaN_3/2 mM MgATP; buffer B, 50 mM imidazole/0.15 M NaCl/2.5 mM $BaCl_2$/1 mM NaN_3/2.5 mM MgATP.

In addition to the already reported orthorhombic crystal form I (15), a monoclinic (form II) and another orthorhombic crystal form (form III) were obtained by mild tryptic treatment of the actin·DNase I complex (Fig. 1). This treatment did not alter the enzymatic activities and the molecular weight of both protein components as judged by electrophoresis on polyacrylamide gels in the presence of sodium dodecyl sulfate. Recently, form III crystals were obtained by using protein not subjected to trypsin digestion.

Heavy-Atom Derivatives. Six heavy-atom derivatives were obtained by soaking form III crystals (see Table 2).

X-Ray Data Collection. Data from native and one derivative crystal form II were collected by using an Arndt–Wonacott oscillation camera (rotating anode, Ni-filtered Cu K_α radiation). For various technical reasons it was decided to suspend work on this crystal form and to continue with the much higher qual-

The publication costs of this article were defrayed in part by page charge payment. This article must therefore be hereby marked "*advertisement*" in accordance with 18 U. S. C. §1734 solely to indicate this fact.

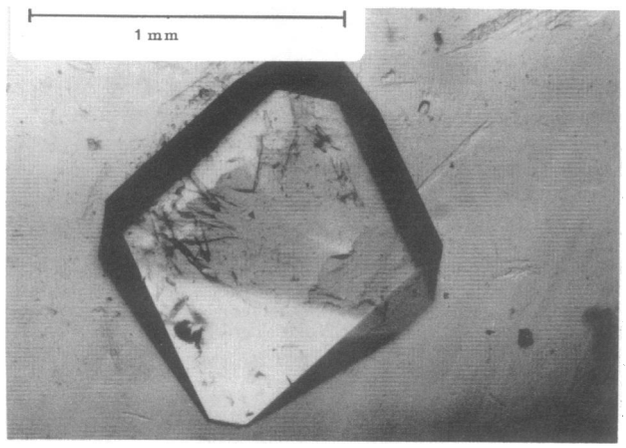

FIG. 1. Form III crystal of actin·DNase I complex. The space group is $P2_12_12_1$ with a = 133.0 Å, b = 56.4 Å, and c = 110.0 Å.

ity type III crystals. X-ray reflection intensities of type III crystals were measured at 7°C by using Ni-filtered Cu K_α radiation with moving-crystal stationary-counter scans on an automatic diffractometer (Syntex, $P2_1$). The typical scan width of a reflection was 0.6° and the scanning time was 1 min. The background was determined by monitoring the intensities at 30 different directions evenly distributed over the measuring triangle by using a $2\theta/\theta$ scan covering the resolution range of the data set. Accidental coincidences with Bragg reflections were corrected by hand. The intensities were corrected for absorption effects by determining the transmission surface of the crystal according to the method of Huber and Kopfmann (16). The intensities of four near-axial reflections were determined in 5° intervals as the crystal was rotated about the corresponding reciprocal lattice vector. The best fit of the observed data was then obtained using a low-order Fourier expansion of the partial transmission. The radiation damage was monitored by measuring the intensities of six standard reflections every 200 reflections and was less than 20% for all data sets.

RESULTS

Crystals. Two new crystal forms (types II and III) were obtained by using mildly trypsin treated actin·DNase I and buffer B. Initially, few type III crystals were observed in a batch of form II crystals. Later on, type III crystals were reproducibly grown by seeding with one or two small crystals. Type III crystals with a slightly altered diffraction pattern also appeared when chicken gizzard actin was used instead of rabbit skeletal muscle actin. The properties of these three crystal forms are summarized in Table 1. In this paper we describe the low-resolution x-ray structure analysis of type III crystals because this crystal form is best suited for x-ray study.

Phase Determination. The phase determination by the isomorphous replacement technique was based on six heavy-atom derivatives. The difference Patterson function of the methylmercuryacetate derivative contained only three prominent peaks on the Harker sections resulting from a single mercury site. The heavy-atom parameters of this site were refined from the 533 independent centric reflections at 6-Å resolution by using a procedure similar to that of Dickerson *et al.* (17). The resulting R_C factor was 42.8% and the phasing power was 2.06. The heavy-atom parameters for the other derivatives were determined from several rounds of cross-difference Fourier syntheses followed by centric parameter refinements. The results of the final simultaneous centric refinement of all derivatives are shown in Table 2. The relatively low mean figure of merit, 0.72, for the 2117 reflections to 6-Å resolution reflects the poor phasing power of the platinum and uranyl derivatives.

Friedel pair intensity differences for the methylmercuryacetate derivative were measured to 8-Å resolution in order to determine the chirality. However, the small correlation coefficient, + 0.25, between calculated and observed differences was considered to be inconclusive.

Electron-Density Map. An electron-density map was calculated by Fourier synthesis using the "best" protein structure factors (18) derived from six heavy-atom derivatives. A contour model was drawn for a whole unit cell in sections of constant y at intervals of $y/28$. As contour levels, 10, 20, ... 90% of the maximum protein density were chosen (Fig. 2). In most regions the boundary of the complex could be traced unambiguously. Only one cut through electron density at the 20% level on a 2_1 axis had to be made. Two further cuts at the 10% level were necessary to separate the asymmetric unit as shown.

The density consists of two clearly distinguishable lobes of different size, suggesting that the larger domain represents actin and the smaller one, DNase I. This assignment is confirmed by a difference Fourier map using a data set of a form III crystal with chicken gizzard actin instead of rabbit skeletal muscle actin complexed with DNase I. Because the sequences of the two actins differ by six amino acid residues (4) the major changes should then appear in the larger domain, which is actually the case.

Further evidence for assignment of the protein density was obtained by locating the two high-affinity Ca^{2+}-binding sites of the DNase I at the surface of the smaller lobe. In contrast to the Ca^{2+}-binding site of actin (19), these sites can also bind Ba^{2+} (20). The localization of these sites was accomplished as follows. In the first experiment, a data set was taken from a crystal soaked in a buffer containing Ca^{2+} instead of Ba^{2+}; in the second experiment, soaking was performed in buffer B containing, in addition, 10 mM EDTA. Both difference Fourier maps showed two prominent negative peaks at identical positions. These positions corresponded to the highest density peaks which lie within the smaller lobe in the native electron density map (Fig. 2). These results are in agreement with biochemical observations indicating that none of the negative peaks in the difference Fourier maps can be due to a loss of ATP bound to actin. It was found that incubation with 10 mM EDTA does not lead to a

Table 1. Crystal data

Crystal form	Space group	Cell constants a, Å	b, Å	c, Å	Habit	Molecules, no./asym. unit	V_M, Å³/dalton	Diffraction limit, Å
I	$P2_12_12$	42.0	230.0	77.0	Needles	1	2.5	4
II	$P2_1$	153.1	42.2	121.9*	Plates	2	2.5	3
III	$P2_12_12_1$	133.0	56.4	110.0	Prisms	1	2.8	2†

* β = 108.1°.
† At 4°C, by using synchrotron radiation.

Table 2. Isomorphous replacement results

Heavy-atom compound	Soaking Conc., M	Soaking Time	R_F, %*	R_C, %†	F_H/E‡	Sites, no.
CH_3HgOAc	10^{-3}	1.5 hr	15.8	48.6	1.8	1
cis-$PtCl_2(NH_3)_2$	10^{-3}	4 days	21.8	64.2	1.2	11
CH_3HgOAc + *cis*	10^{-3}	1.5 hr	26.3	69.2	1.0	11
$PtCl_2(NH_3)_2$	10^{-3}	5 day				
Uranyl acetate	10^{-3}	6 day	8.5	75.9	0.8	2
K_2PtCl_4	10^{-4}	6 day	23.5	72.3	1.0	3
$NaReO_4$	10^{-2}	9 day	12.9	63.1	1.2	1

Mean figure of merit for all reflections, $m = 0.72$.
* $R_F = \{\Sigma||F_{PH}| - |F_P||\}/\Sigma|F_P|$.
† Cullis R factor for centric reflections.
‡ Phasing power.

release of the fluorescent ATP analogue etheno-ATP from the complex (ref. 9; unpublished results).

Because DNase I contains two S-S bridges but no free SH group, the mercury position derived from the methylmercury-acetate derivative most probably marks one of the accessible SH groups of actin. In agreement with the evidence mentioned above, this mercury position is located within the large domain.

A balsa wood model was carved to include density above 10% of the maximal electron density in the map. The molecular weight of the actin·DNase I complex was estimated from this balsa wood model to be 73,000 (21) which compares well with the sum of the molecular weights 42,000 for actin (3) and 31,000 for DNase I (12) calculated from the known amino acid sequences. However, estimating the molecular weights of the large and small lobes by the same method, we obtain 50,000 and 23,000, respectively. This means that some density of the larger lobe must be part of DNase I.

Because there are only two thin connections between the two lobes, any cutting through the large lobe would lead to a strange molecular shape for DNase I. Furthermore, the high affinity constant of the actin·DNase I complex (9) could hardly be explained with such a small contact area between the two components. Therefore, it was decided to redefine the asymmetric unit by cutting these two thin connections and considering a crystallographically equivalent smaller lobe related to the original one by the 2-fold screw axis between the two density regions, as shown in Fig. 2. This immediately leads to a more compact form of the complex (Fig. 3) and both its components and allows in addition a cutting in proportion of their molecular weights.

The complex has dimensions 87 × 67 × 43 Å. The actin molecule is elongated and consists of a large and a small domain with overall dimensions of 67 × 40 × 37 Å (Fig. 4). Both domains contain density regions which resemble a central β-pleated sheet surrounded by two or three α-helices near the surface of the molecule. The highest electron density occurs in the cleft between the two domains, suggesting that this density might represent ATP (Fig. 2). This agrees with our observations for elongation factor Tu·GDP at 6-Å resolution (21) in which the highest density turned out to be the bound nucleotide (22).

The DNase I molecule has dimensions 50 × 50 × 40 Å and contains a few rod-like features but appears to be less compact than actin. The location of the two Ca^{2+}-binding sites at the surface of the molecule and the fact that Ca^{2+} can be replaced by Ba^{2+} resembles somewhat the situation found for two of the four Ca^{2+} in thermolysin (23).

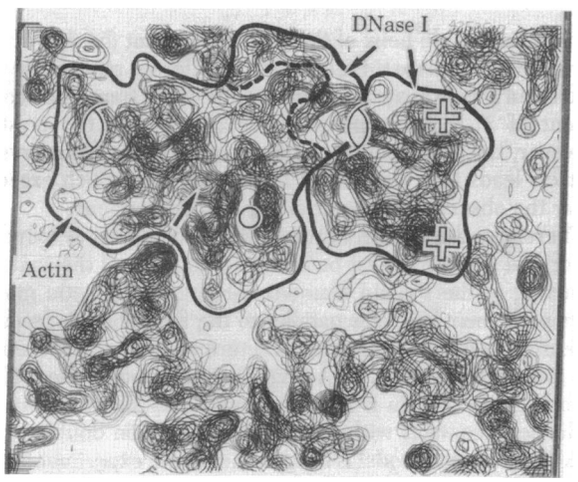

FIG. 2. Sections 19/28 to 27/28 perpendicular to the *b* axis of the electron density of a full unit cell of rabbit skeletal muscle actin·DNase I complex. The distance between sections is 2Å. Contours are drawn at intervals of 10% of the maximal density. The content of one asymmetric unit is enclosed by solid black lines. The smaller density region on the right-hand side represents DNase I. The density encircled on the left side is mostly attributed to actin. The proposed boundary between actin and DNase I is indicated by the broken line. To obtain the complex shown in Fig. 3, the DNase I density on the right side of the picture must be transformed by the crystallographic 2-fold screw-axis ( ) between the two density regions. ○, Position of the mercury atom bound to actin is marked by a circle; + Ca^{2+} positions in the DNase I are indicated by crosses; arrow, the highest density peak in the actin molecule, presumably representing ATP. The only contact found between actin monomers occurs on the 2-fold screw-axis shown in the left part of the figure.

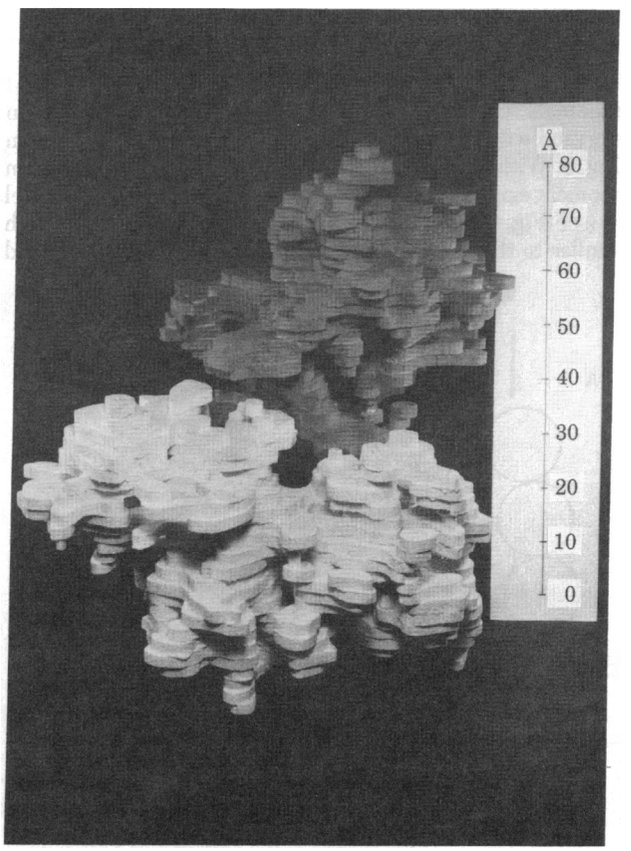

FIG. 3. Balsa wood model of the actin·DNase I complex at 6-Å resolution. The lower part of the model represents actin. The cutting level is 10% of the maximal electron density.

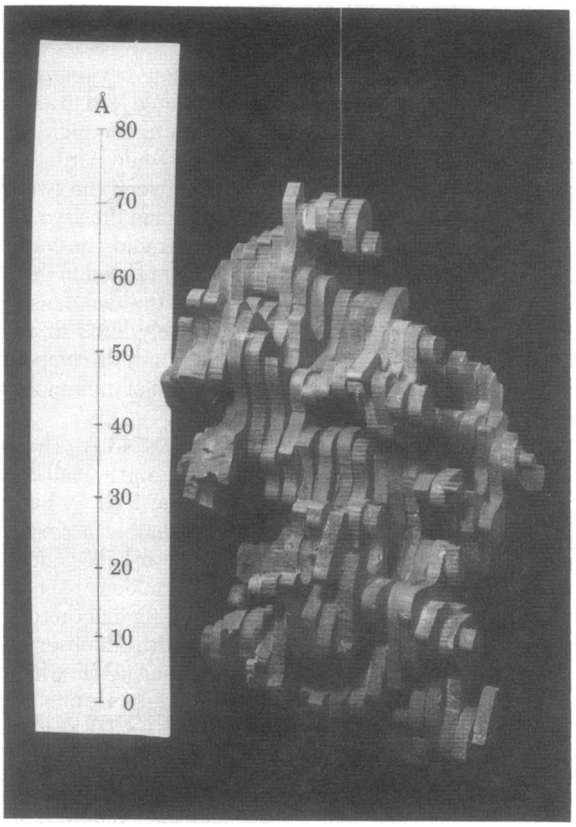

FIG. 4. Balsa wood model of the actin molecule at 6-Å resolution. The molecule is elongated with overall dimensions 67 × 40 × 37 Å and consists of a larger and a smaller domain.

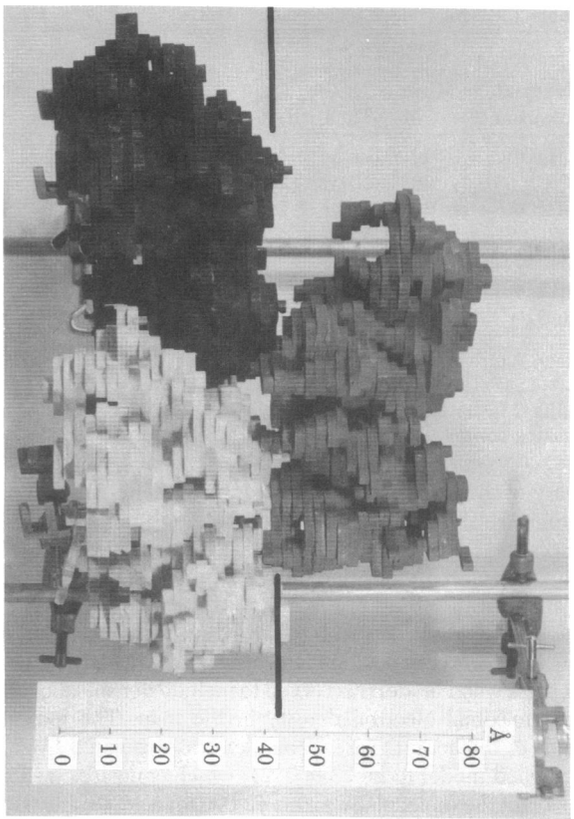

FIG. 6. Balsa wood models of three actin molecules as derived from the electron-density map arranged in agreement with the observed geometry of the F-actin filament. The filament axis is indicated by the black lines. The two models on the left belong to the same strand.

DISCUSSION

A schematic comparison of the packing of actin monomers in the crystal with the F-actin filament (e.g., see ref. 24) is given in Fig. 5. Within the crystal the only close contact between actin monomers exists on a crystallographic 2-fold screw axis parallel to *b* (see Fig. 2). The repeat distance along *b* is 56.4 Å which is similar to the separation of actin monomers within a strand of the actin double helix of the F-actin filament (54.6 Å). Furthermore, adjacent actin molecules in different strands are related by an approximate 2-fold screw axis with a translation component of 27.3 Å compared to 28.2 Å within the crystal. However, the arrangement of actin monomers by using crystal contacts leads to a filament of 120-Å diameter which exceeds by far the observed diameter of the F-actin filament.

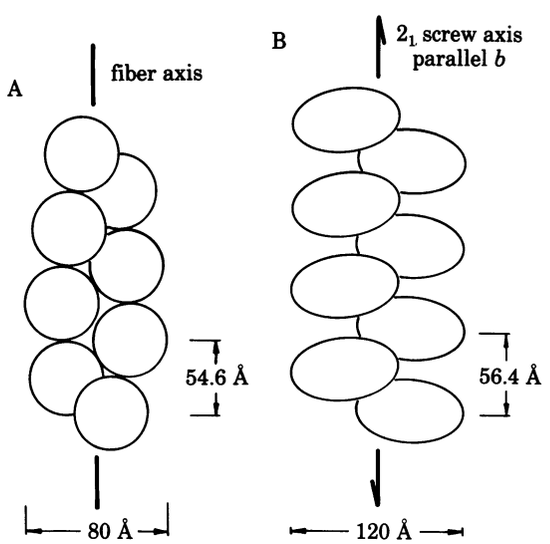

FIG. 5. Comparison of packing of G-actin in the crystal with the F-actin filament. (*A*) Arrangement of actin monomers in the actin filament. (*B*) Crystal packing of actin molecules along a 2-fold screw axis parallel to *b*.

Therefore, the contact between actin monomers as found in the crystal structure must be different from any of the contacts occurring in the F-actin filament. Arranging the actin monomers with their long axis parallel to the filament axis leads to a possible model of the F-actin structure with the correct repeat and a diameter of about 80 Å (Fig. 6). In this model the DNase I binding site of actin is accessible with only slight distortions of the actin contacts within a strand of the actin double helix. This feature of the model is in agreement with experiments suggesting that DNase I can also bind to F-actin, although with a lower affinity than to G-actin (8, 9).

The molecular dimensions of the actin monomer (67 × 40 × 37 Å) as determined from this 6-Å x-ray analysis are larger than those derived from electron microscopy studies. Aebi *et al.* (25) examined crystalline actin sheets and reported an elongated form of the molecule measuring 56 × 33 Å in projection. This is in reasonable agreement with our results, in particular if we compare the ratios between the long and short dimensions, 67 Å:38.5 Å = 1.74 and 56 Å:33 Å = 1.70, respectively. Furthermore, their observation of a major and a minor peak of the projected mass density along the long axis of the molecule is in qualitative agreement with our model. From three-dimensional image reconstructions of actin-tropomyosin filaments, Wakabayashi *et al.* (26) derived molecular dimensions of about 45

× 30 × 25 Å for the actin monomer. As they discussed, these numbers are expected to be too small because of shrinkage during the staining procedure.

We thank H. Pfrang for excellent technical assistance, Dr. E. Novak for kindly supplying us with chicken gizzard actin, and Dr. K. C. Holmes for his interest and helpful discussions. H.G.M. thanks the Deutsche Forschungsgemeinschaft for financial support.

1. Pollard, T. D. & Weihing, R. R. (1974) *Crit. Rev. Biochem.* **2,** 1–65.
2. Clarke, M. & Spudich, J. A. (1977) *Annu. Rev. Biochem.* **46,** 797–822.
3. Elzinga, M., Collins, J. H., Kuehl, W. M. & Adelstein, R. S. (1973) *Proc. Natl. Acad. Sci. USA* **70,** 2687–2691.
4. Vandekerckhove, J. & Weber, K. (1979) *FEBS Lett.* **102,** 219–222.
5. Mannherz, H. G. & Goody, R. S. (1976) *Annu. Rev. Biochem.* **45,** 427–465.
6. Carlsson, L., Nyström, L.-E., Lindberg, U., Kannan, K. K., Cid-Dresdner, H., Lövgren, S. & Jörnvall, H. (1976) *J. Mol. Biol.* **105,** 353–366.
7. Mannherz, H. G., Barrington-Leigh, J., Leberman, R. & Pfrang, H. (1975) *FEBS Lett.* **60,** 34–38.
8. Hitchcock, S. E., Carlsson, L. & Lindberg, U. (1976) *Cell* **7,** 531–542.
9. Mannherz, H. G., Goody, R. S., Konrad, M. & Nowak, E. (1980) *Eur. J. Biochem.* **104,** 367–379.
10. Rohr, G. & Mannherz, H. G. (1978) *Eur. J. Biochem.* **89,** 151–157.
11. Burgoyne, L. A., Wagar, M. A. & Atkinson, M. R. (1970) *Biochem. Biophys. Res. Commun.* **39,** 254–259.
12. Liao, T.-H., Salnikow, J., Moore, S. & Stein, W. H. (1973) *J. Biol. Chem.* **248,** 1489–1495.
13. Salnikow, J., Moore, S. & Stein, W. H. (1970) *J. Biol. Chem.* **245,** 5685–5690.
14. Strzelecka-Golaszewska, H., Prochniewicz, E., Nowak, E., Zmorzynski, S. & Drabikowski, W. (1980) *Eur. J. Biochem.* **104,** 41–52.
15. Mannherz, H. G., Kabsch, W. & Leberman, R. (1977) *FEBS Lett.* **73,** 141–143.
16. Huber, R. & Kopfmann, G. (1969) *Acta Crystallogr.* **A25,** 143–152.
17. Dickerson, R. E., Weinzierl, J. E. & Palmer, R. A. (1968) *Acta Crystallogr.* **B24,** 997–1003.
18. Blow, D. M. & Crick, F. H. C. (1959) *Acta Crystallogr.* **12,** 794–802.
19. Kasai, M. & Oosawa, F. (1968) *Biochim. Biophys. Acta* **154,** 520–528.
20. Price, P. A. (1975) *J. Biol. Chem.* **250,** 1981–1986.
21. Kabsch, W., Gast, W. H., Schulz, G. E. & Leberman, R. (1977) *J. Mol. Biol.* **117,** 999–1012.
22. Suck, D. & Kabsch, W. (1981) *FEBS Lett.* **126,** 120–122.
23. Matthews, B. W., Colman, P. M., Jansonius, J. N., Titani, K., Walsh, K. A. & Neurath, H. (1972) *Nature (London) New Biol.* **238,** 41–43.
24. Moore, P. B., Huxley, H. E. & DeRosier, D. J. (1970) *J. Mol. Biol.* **50,** 279–295.
25. Aebi, U., Smith, P. R., Isenberg, G. & Pollard, T. D. (1980) *Nature (London)* **288,** 296–298.
26. Wakabayashi, T., Huxley, H. E., Amos, L. A. & Klug, A. (1975) *J. Mol. Biol.* **93,** 477–497.